Article

Projections of Changes in Atmospheric Conditions Leading to Storm Surges along the Coast of Santos, Brazil

Marcely Sondermann [1,*], Sin Chan Chou [1], Priscila Tavares [1], André Lyra [1], José A. Marengo [2] and Celia Regina de Gouveia Souza [3]

1 National Institute for Space Research, Cachoeira Paulista 12630-000, SP, Brazil; chou.chan@inpe.br (S.C.C.); priscila.tavares@inpe.br (P.T.); andre.lyra@inpe.br (A.L.)
2 National Center for Monitoring and Early Warning of Natural Disasters (CEMADEN), São José Dos Campos 12247-016, SP, Brazil; jose.marengo@cemaden.gov.br
3 Institute of Environmental Researches, Secretariat for the Infrastructure and Environment of the State of São Paulo, São Paulo 05508-090, SP, Brazil; celia@sp.gov.br
* Correspondence: marcely.silva@inpe.br

Abstract: This study aims to assess the changes in the atmospheric conditions favorable to storm surges over the Santos Coast in Southeast Brazil. Storm surges can favor high sea level rises and coastal erosion, affecting people and strategic structures in coastal areas. The assessment of the atmospheric conditions was based on the downscaling of climate simulations of the Brazilian Earth System Model by the Eta regional climate model at higher spatial resolution. The detection scheme used by the model was able to reproduce the three observed atmospheric patterns favorable to storm surges found by recent studies: Pattern 1 is characterized by a cyclone on the synoptic scale over the ocean; Pattern 2 presents an intense wind fetch from the southeast; Pattern 3 is characterized by winds parallel to the coast. The simulations underestimated the number of cases in Patterns 1 and 2. However, it overestimated the number of days in Pattern 3. The model presented more intense winds in the three patterns. The storm surges characterized by Pattern 1 will become more intense. However, it will be equal to or less frequent. In Pattern 2, the number of events will decrease. Nevertheless, these episodes will be associated with more precipitation along the coastline. Pattern 3 will have a similar number of storm surges.

Keywords: Eta Model; climate change; coastal hazards

1. Introduction

Storm surge is the temporary increase, at a particular locality, in the height of the sea due to extreme meteorological conditions, according to the Special Report on the Ocean and Cryosphere in a Changing Climate (SROCC). The authors of [1] define storm surges as rising sea levels due to low atmospheric pressure and strong winds. In addition, these authors conclude that tropical cyclones drive the most extreme storm surges. However, extratropical cyclones can also be responsible for high sea levels, especially when they coincide with high tides [2].

Coastal zones are considered highly vulnerable to climate change effects, including sea level rise [3], changes in the frequency and intensity of storms [4], increases in precipitation, and warmer ocean temperatures. Furthermore, most of the world's coastal regions in which intense storms pass on a regular or occasional basis are affected by storm surges [5]. In addition, the concurrent events of heavy precipitation and storm surges are increasing in coastal areas worldwide, according to the analyses of past changes observed by the authors of [6].

In [7], the authors identify the atmospheric conditions favorable to causing storm surges on the coast of Santos from May 1981 to 2010. In addition, they verify that the number of storm surge events and the maximum monthly significant wave height is increasing during May. These diagnostics are obtained using ERA5 reanalysis data [8]. The choice of May is

associated with a higher frequency of storm surges in Southeast Brazil between April and September [7,9,10]. Ref. [9] show a historical analysis based on an observational database of Santos. They conclude that May and July have the highest storm surge events. In addition, May presents the highest wave heights during storm surges, according to these authors.

The projected changes in the frequency of extreme winds are associated with the changes in the characteristics (locations, frequencies, and intensities) of tropical and extratropical cyclones [11]. These changes could contribute toward increasing or decreasing future storm surge risk.

Future projections of climate change over the city of Santos, including the trend of temperature, precipitation, indicators of climatic extremes, and storms related to extratropical cyclones, are evaluated in [12] based on the downscaling of three global climate models at the RCP4.5 and RCP8.5 scenarios. The assessment of climate change projections indicates warming, about 2 °C by the end of the 21st century, and a reduction in rainfall across the region. The projections of the minimum surface pressure over the coast of southeastern Brazil showed a weakening trend in the RCP8.5 scenario. These results may contribute to a change in the characteristics of the intensity and frequency of storm surge events in that region.

The main goal of this study is to assess the changes in the atmospheric conditions favorable to cause storm surges in the future climate. The frequency and duration of atmospheric conditions favorable to storm surge over the Coast of Santos, in Southeast Brazil, are assessed. This information on the changes in the atmospheric conditions prone to storm surges is expected to support the studies on impact, vulnerability, and adaptation to climate change in the coastal area of Santos.

2. Materials and Methods

The assessment of the atmospheric conditions was based on the downscaling of climate simulations of the Brazilian Earth System [13] using the Eta regional climate model [14,15] at higher spatial resolution. The study region, the BESM, and the Eta Model are described below.

2.1. The Study Region

Santos is a coastal city in São Paulo State, Southeastern Brazil (Figure 1). The population is 432.957 [16] in an area of approximately 280.000 km^2. This region has several economic activities, such as tourism and the presence of the Port of Santos, one of the largest ports in Latin America, with a large concentration of industries and expensive housing located along the coastal zone.
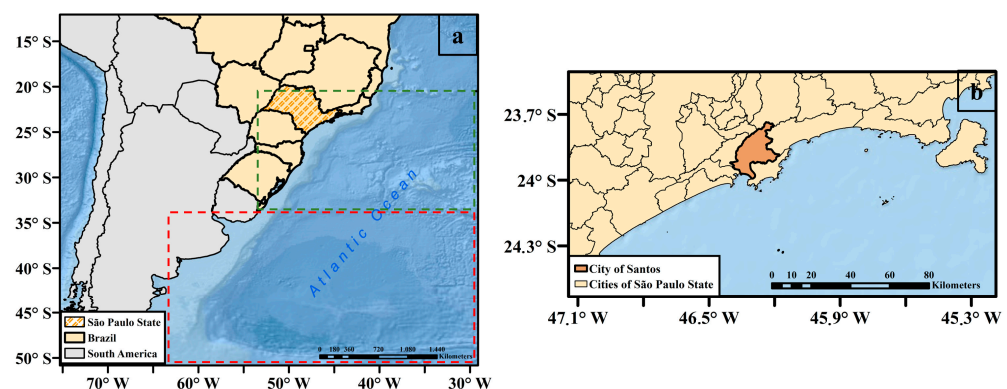

Figure 1. (**a**) Area 1 (green dashed box) and Area 2 (red dashed box), where mean values of mean sea level pressure, wind speed, and wind direction at 10 m are taken. (**b**) The coastal area of Sao Paulo and the city of Santos are more detailed.

Santos is vulnerable to occurrences of extreme meteorological and oceanographic events, such as storms, strong winds, and heavy precipitation, which can cause floods and landslides [16,17]. In this region, the main cause of storms is the presence of extratropical cyclones associated with frontal systems, often with strong southwest winds that blow parallel to the

coast. Therefore, past and future climate conditions are analyzed to support studies on the impacts, vulnerability, and adaptation measures to climate change in this region.

2.2. Eta Model

The regional climate model adopted for higher-resolution downscaling is the Eta Model. This model is a grid-point limited area. One of the characteristics of the model is the eta vertical coordinate [18], which represents the topography in steps. The approximately horizontal surfaces of the coordinate reduce errors in calculating the horizontal derivatives, particularly the horizontal pressure gradient force. Therefore, the eta coordinate is especially suitable for operating in regions of steep topography. A cut-cell feature was added to the orography to allow slanted flow near mountain tops [19,20].

The Eta is a model with full dynamics and physics. The climate version [21–23] operated only in hydrostatic mode. The non-hydrostatic modifications followed in [24] and the results of this version were evaluated in [15] using simulations of Southeast Brazil at 5 km resolution.

The model equations are solved using the Arakawa E-grid. The time integration is split-explicit, using the forward–backward and Euler–backward schemes modified by the authors of [25]. The horizontal advection follows the Arakawa approach [26], and the vertical advection uses the piecewise linear scheme, which makes it a full finite volume model [19]. The model physics package of the climate version applies the Betts–Miller scheme [27] to produce convective precipitation and the Zhao scheme [28] for grid-scale precipitation. The longwave component of the radiation is solved in [29], and the shortwave component is solved in [30]. The surface layer is based on the Monin–Obukhov similarity theory and stability functions [31]. Land-surface processes are treated using the NOAH scheme [32]. The turbulence parameters follow [33].

Climate change simulations from regional climate models are helpful for the assessment of impacts due to the local scale and the magnitude of the changes. Improving orography descriptions and other surface characteristics helps to detail the climate system. However, the climate reproduced by a regional climate model is strongly dependent on the lateral boundaries.

In this study, the Eta regional model [14] is nested into the Brazilian Earth System Model (BESM) global model [13,34] developed by the National Institute for Space Research (INPE). The nested simulations are referred to as Eta-BESM. The model has results using two domains, one that covers South America at 20 km resolution and another that covers Southeastern Brazil at 5 km resolution. This version of the Eta model is adapted for climate change studies [15].

In this study, the present climate (reference period) is simulated from 1976 to 2005, whereas the future climate is projected for 2031 to 2060 under the RCP4.5 and RCP8.5 emission scenarios.

The 5 km resolution non-hydrostatic Eta runs were driven by the 20 km resolution Eta simulations via the lateral boundaries. The 20 km Eta runs are, in turn, driven by the BESM. Therefore, the 5 km Eta runs are the second nesting of the BESM runs.

The sea surface temperature is derived from the BESM and updated daily. Initial soil moisture and soil temperatures are derived from the BESM. Lateral boundaries are updated every 6 h. The model has 38 vertical layers, with the model top at 25 hPa.

2.3. Atmospheric Patterns in Storm Surge

Ref. [7] described three atmospheric patterns that favor the occurrence of storm surges on the coast of São Paulo based on sea level pressure, wind speed, and direction, using ERA5 data for May, from 1981 to 2010. Eighty-nine storm surge days were found and clustered into three patterns.

Pattern 1 (Figure 2a) is characterized by a very intense low-pressure center near the coastline. The wind blows from the southwest and parallel to the coast. There are no expressive rainfall values on the Santos coast.
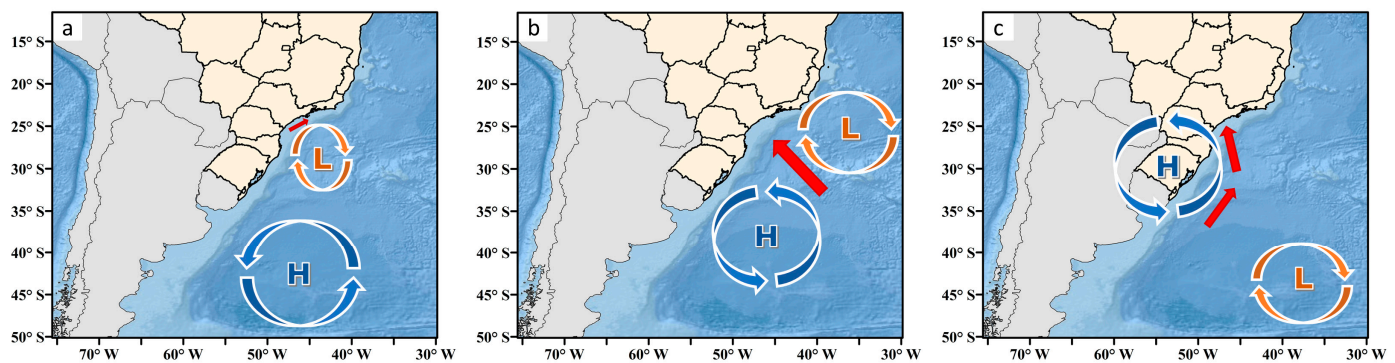
Figure 2. Atmospheric patterns favorable to storm surge events: (**a**) Pattern 1, (**b**) Pattern 2, and (**c**) Pattern 3. "H" is high pressure, and "L" is low pressure. The red arrow is associated with the maximum wind speed and its direction. Adapted from [7].

Pattern 2 (Figure 2b) is characterized by the long and wide wind fetch created by a high-pressure center south of the South Atlantic Ocean and a low-pressure center north of the South Atlantic Ocean. This pattern is associated with a large area of intense winds, allowing a more efficient propagation of high ocean waves. In addition, the winds carry moisture from the ocean towards the coast, contributing to more significant rainfall along the Santos coast.

Pattern 3 (Figure 2c) is characterized by southwesterly winds blowing from high pressure centered over the continent and elongated low pressure over the ocean. Hence, the atmospheric horizontal pressure gradient caused by these pressure centers produces intense southerly winds along the coastline, favoring high waves in this region. Nevertheless, the downward vertical motion of the high-pressure system results in dry regions, inhibiting convective motion and affecting rain formation.

2.4. Detecting Atmospheric Patterns in Storm Surge

The daily outputs of the 20 km Eta model simulations are compared to the three patterns described in the previous section. The comparison is made for May of the reference period from 1976 to 2005 and of the future climate from 2031 to 2060.

To detect the storm conditions in the long climate simulations, we apply pattern correlation of the mean sea level pressure of areas 1 and 2, shown in Figure 1a, and the zonal and meridional components of the 10 m wind over Area 1. We can consider a day with favorable atmospheric conditions for a storm surge when the spatial correlation of the three atmospheric variables, i.e., mean sea level pressure, wind speed, and wind direction, is greater than or equal to 0.5. From this, the possible days with potential for storm surge belonging to each pattern are detected.

The same is performed to detect the conditions required for the occurrence of storm surges in the future, from 2031 to 2060, under RCP4.5 and RCP8.5 emission scenarios.

Global climate models (GCMs) are essential for improving and understanding global climate change. In general, the resolution of GCMs is coarse to capture details in these studies. On the other hand, the impacts in different socioeconomic sectors occur at a local scale. Therefore, regional climate models of smaller grid sizes are required to improve over the GCM driver and capture a phenomenon's intensity more accurately. Thus, a higher resolution is needed to study the impacts at the urban coastal scale.

To assess the local impacts of the storm surges around the coastal area, a second level of downscaling of 5 km resolution Eta-BESM was performed. This resolution is more suitable for reproducing regional climate details in the metropolitan and Santos' coastal regions. Therefore, the refinement produced by the regional climate model in the highest resolution is essential to improve the quality of data and information. In addition, improving the coastline description is particularly important for the present study.

Spatial patterns of atmospheric variables, such as mean sea level, wind at 10 m, and precipitation in storm surge potential days, are produced by the 20 km Eta. An evaluation of local impacts in the coastal zone of Santos by the 5 km Eta is also performed. In addition, both results are compared to show the improvements of a higher resolution.

3. Results

In this section, the three surface atmospheric patterns favorable to the occurrence of storm surges simulated by the 20 km Eta-BESM model for the reference climate (1976–2005) and for the future climate (2031–2060) are presented.

In addition, the atmospheric conditions projected by 5 km Eta-BESM for the future climate from 2031 to 2060, using only one greenhouse gas emission scenario, RCP8.5, are also analyzed.

3.1. Large-Scale Atmospheric Patterns

3.1.1. Reference Climate

In May, from 1976 to 2005, the 20 km Eta-BESM simulated a total number of 99 days with the potential to form a storm surge near the coast of Santos. Therefore, the simulations overestimate the number of potential storm surge days; the number of days in 30 years of the ERA5 dataset identified was 89 [7].

The mean of each meteorological pattern simulated by the 20 km Eta-BESM from 1976 to 2005 is presented in (Figure 3).
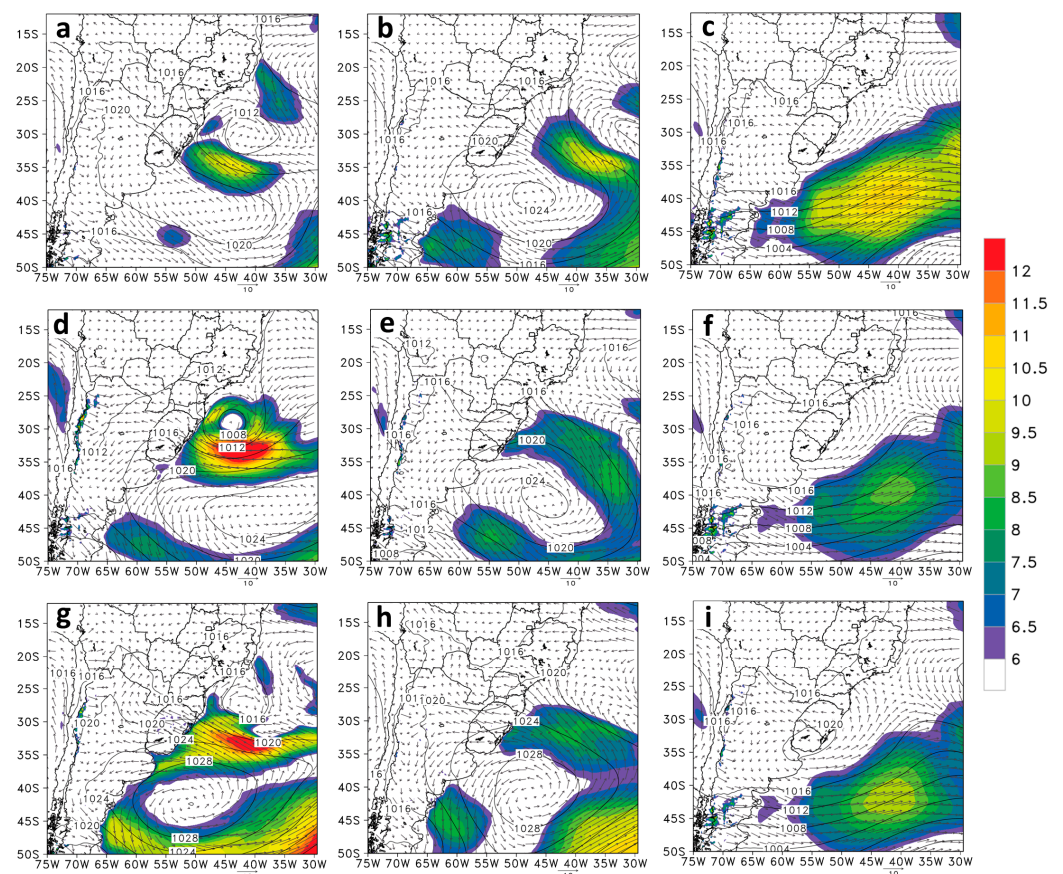

Figure 3. The three patterns of intensity and wind direction at 10 m (shading and vectors, respectively) and PNMM (isolines) favorable to the occurrence of storm surges simulated (**a**–**c**) to the reference period (1976–2005) and projected by the 20 km Eta-BESM in May during the future cli-mate (2031–2060), using RCP4.5 (**d**–**f**) and RCP8.5 (**g**–**i**): Pattern 1 (first column); Pattern 2 (second column); and Pattern 3 (third column).

Pattern 1 (Figure 3a) presents a lower pressure center between the South and Southeast Regions with southwest winds parallel to the coast. The wind speed on the coast is less than 6 m/s; in contrast, the ERA5 Reanalysis shows a wind speed greater than 8 m/s. Pattern 1 presents the least number of days; the ERA5 Reanalysis had 10 days, whereas the simulation detected 5 potential days.

Pattern 2 (Figure 3b) reproduces a more intense wind fetch than the ERA5 Reanalysis. The maximum wind speed is around 11 m/s. This wind fetch is formed by the presence of a high-pressure center, located approximately at 40° S and 47° W, and a low-pressure center at 30° S and 30° W. The simulation detects 15 potential days of storm surge. Therefore, it underestimates the number of days compared to the ERA5 Reanalysis, which is 22 days.

Pattern 3 (Figure 3c) presents the southwesterly winds from the higher pressure over the continent. There is also a trough over the ocean with wind speeds greater than 14 m/s. Therefore, the wind speed is overestimated in this region compared to the ERA5 Reanalysis, which reaches 8 m/s. The simulation reproduces 79 potential days, a large number compared to the 57 potential days from the ERA Reanalysis. Similar to the reanalysis, the simulation shows that this pattern is the most frequent.

3.1.2. Future Climate

The assessment of future hazards in coastal cities requires knowledge about projections of future storms and storm surges. The total number of storm surges projected using the RCP4.5 was 91, whereas the RCP8.5 detected 84 days. Both scenarios indicate a decrease in potential storm surge days concerning the reference climate. The projections are shown in Figure 3 (second and third rows).

Pattern 1 contains the least number of potential days in both scenarios. The RCP4.5 (Figure 3d) shows 5 days, whereas the RCP8.5 (Figure 3g) shows only one day. The RCP4.5 scenario projects a low pressure near the coast, and the center value is 1008 hPa. It is more intense than in the reference climate, and its center value is 1012 hPa. In contrast, the RCP8.5 scenario shows a low center pressure equal to 1016 hPa. In addition, the winds parallel to the Santos coast are stronger in RCP4.5.

The RCP4.5 (Figure 3e) scenario projected in Pattern 2 presents a more intense fetch wind compared to the RCP8.5 (Figure 3h) scenario. In RCP4.5, the values are greater than 6 m/s. In both scenarios, there is a decrease in wind speed in comparison with the reference climate. The mean sea level pressure values simulated by RCP8.5 are higher than the reference period. Therefore, there is a more intense high-pressure center over the continent and a less intense low-pressure center over the ocean in the simulated future.

Pattern 3, in RCP4.5 (Figure 3f), presents the high-pressure center of 1016 hPa over the continent, whereas in RCP8.5 (Figure 3i), the pressure center is 1020 hPa, which is more intense than the 1016 hPa of the reference climate. In both scenarios, the wind speed is greater in the trough area over the ocean, and the maximum values range from 8 to 10 m/s. However, these wind speeds are weaker than those of the reference climate when they were around 12 m/s.

3.2. *Local Impacts Simulated by 5 km Eta Model*

To assess the impacts of climate change on the storm surges near the coast of Santos, higher spatial resolution is required as the coastal processes have local scale features. The high-resolution dynamic downscaling, the 5 km Eta-BESM, is produced to evaluate the local impacts of atmospheric conditions in potential storm surge days on Santos Coast reproduced by the 20 km Eta-BESM. At higher spatial resolution, a detailed land cover description is necessary to capture the small-scale variability [15].

3.2.1. Reference Climate

The three meteorological patterns required for storm surges simulated to the reference climate (1976–2005) by the 5 km Eta-BESM are shown in Figure 4.
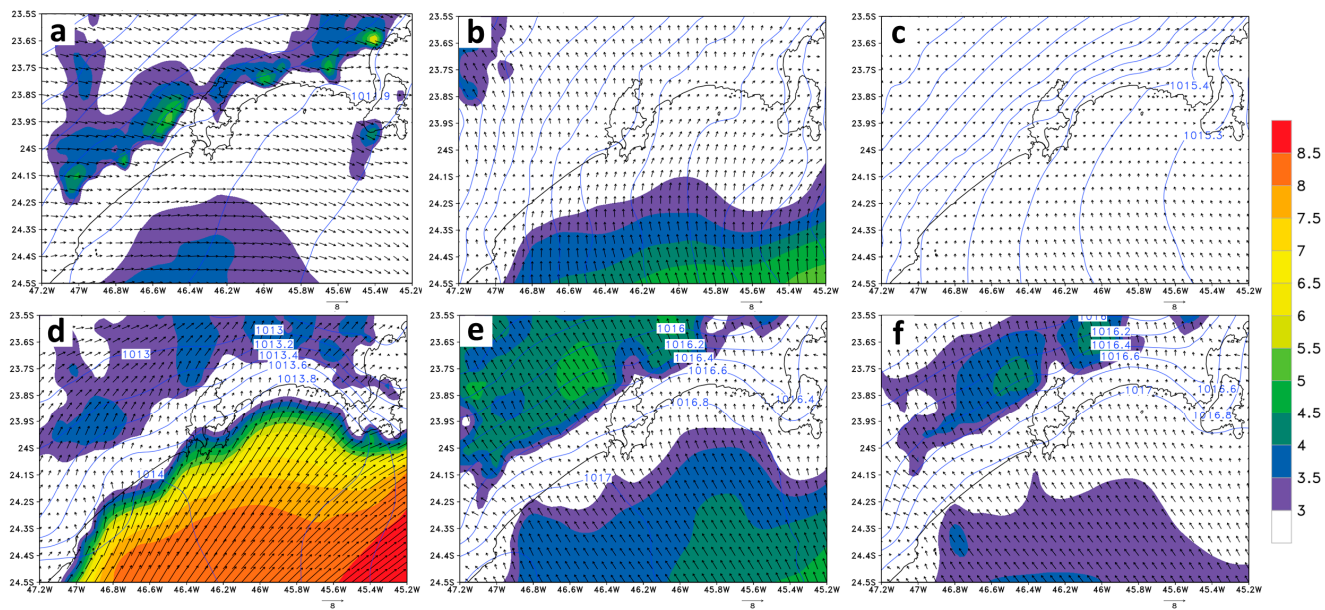
Figure 4. The three local patterns of intensity and wind direction at 10 m (shading and vectors, respectively) and PNMM (isolines) favorable to the occurrence of storm surges simulated to the reference period (1976–2005) by the 20 km Eta-BESM in May at 06Z (**a**–**c**) and 18Z (**d**–**f**): Pattern 1 (first column); Pattern 2 (second column); and Pattern 3 (third column).

Mean Sea Level Pressure and 10 m Wind

Frontal systems and breeze circulation influence Santos and orography [35]. To capture the signal of the diurnal cycle and the breeze circulations, we analyzed the outputs at 06Z and 18Z. These local circulations are driven by thermal and pressure differences between two different land covers. At 06Z, which is 03LT, nighttime, the land breeze blows from continent to ocean (northwest–southeast), while at 18Z, which is 15LT, the wind blows from ocean to continent (southeast–northwest) in the sea breeze. On the other hand, the synoptic-scale weather systems in storm surge events overlap the breeze effects.

Pattern 1 is characterized by a cyclone on the synoptic scale, over the ocean, with parallel winds on the coast. In the 5 km simulation at 06Z (Figure 4a), the winds from the southwest are weakened due to the force of the pressure gradient of the land breeze circulation, which presents winds with a direction opposite (northwest winds) to the large-scale flow. At 18Z (Figure 4d), the pressures decrease from the ocean to the continent, and the wind flux happens from higher to lower pressures. Combined, this flux and the sea breeze accelerate the surface flow towards the coastal region.

Pattern 2 presents an intense wind fetch from the southeast, created by an anticyclone and a cyclone over the ocean on a synoptic scale, extending to Santos's coastal region. At 06Z (Figure 4b), the 10 m winds near the coast exceed 3 m/s. The predominant wind directions are from the south and southeast. Therefore, large-scale circulation prevails over the land breeze. At 18Z (Figure 4e), the sea breeze contributes to the same direction, from the southeast, to accelerate the large-scale flux.

Pattern 3 is the most frequent and favorable to storm surges. It is characterized by winds parallel to the coast from a high-pressure center over the continent. On a local scale, at 06Z (Figure 4c), southwesterly winds weaken as they approach the coastal zone, which may occur due to the roughness of the land and topography that acts to slow them down. At 18Z (Figure 4f), the winds are from the southeast, which is favored by the circulation of the sea breeze.

Precipitation

The precipitation (mm/day) to the three atmospheric patterns required to storm surges in the reference climate are shown in Figure 5. The observed rain from MSWEP [36] to

storm surge days selected by the ERA5 Reanalysis are presented in the first line. The simulations by the 5 km Eta-BESM are shown in the second line. Finally, the results from the 20 km Eta-BESM are presented in the last line.
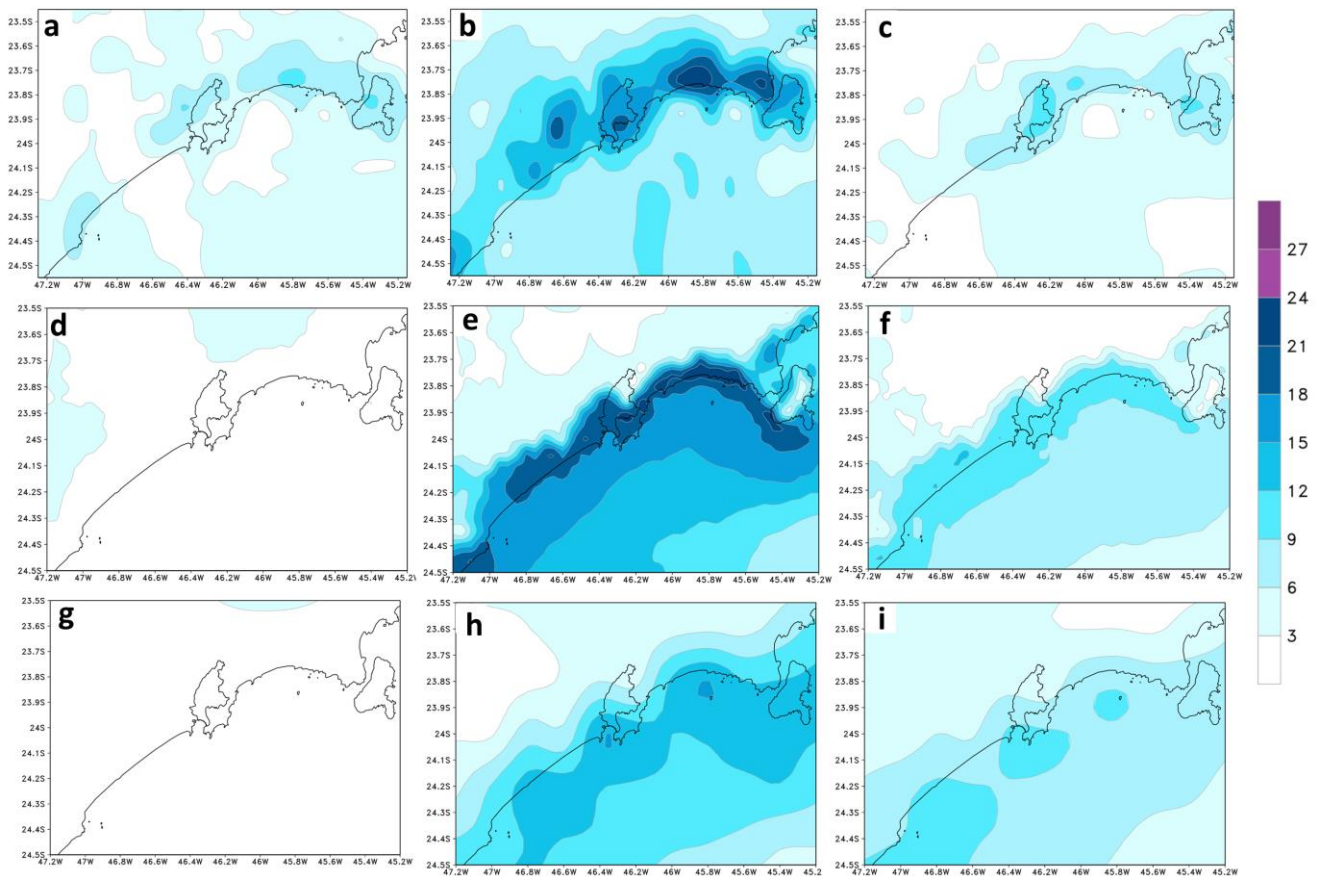

Figure 5. The three rainfall patterns favorable to the occurrence of storm surges from the MSWEP (1981–2000; (**a–c**)), simulated by the 5 km Eta-BESM (1976–1995; (**d–f**)) and by the 20 km Eta-BESM (1976–1995; (**g–i**)) in May over the city of Santos: Pattern 1 (first column); Pattern 2 (second column); and Pattern 3 (third column).

Statistical dependence between extreme rainfall and storm surge is likely as common meteorological forcing often drives both variables. Cyclonic systems may produce strong onshore winds leading to an extreme storm surge while generating large amounts of rainfall on the adjacent coastal catchments [37].

Pattern 1 (Figure 5d) presents values less than 3 mm/day on the coast. Although this pattern presents a cyclone on the coast, this is the least rainy. The simulation by the 5 km Eta-BESM underestimates the precipitation.

In contrast, Pattern 2 accumulates more precipitation. The simulations by the 5 km Eta-BESM (Figure 5e) show precipitation rates greater than 21 mm/day alongshore, which is overestimated according to MSWEP observations. This precipitation is a response to the intense wind fetch that brings moisture from the ocean to the continent and causes heavy rain.

The Pattern 3 (Figure 5f) simulations reproduce the maximum precipitation along the coast at rates closer to the MSWEP precipitation observations, although still overestimating. The simulations show precipitation rates greater than 12 mm/day alongshore. The largest precipitation amount in this region is related to the southwesterly winds from the high pressure over the continent on a large scale. This high-pressure system contributes to moisture transport at lower levels from the ocean toward the coast.

Generally, the 5 km Eta-BESM (Figure 5d–f) produces more rain than the 20 km Eta-BESM (Figure 5g–i) over the region. Despite that, both simulations agree with the rain distribution in the three patterns: the least precipitation in Pattern 1 and the most in Pattern 2.

3.2.2. Future Climate

Mean Sea Level Pressure and 10 m Wind

The climate future projections (2031–2060) over the scenario RCP8.5 by the 5 km Eta-BESM are shown in Figure 6. This figure presents the wind speed difference between the future and the reference climate to the three atmospheric patterns required to storm surge at 06Z and 18Z. However, the wind direction and sea-level pressure are in the future climate.
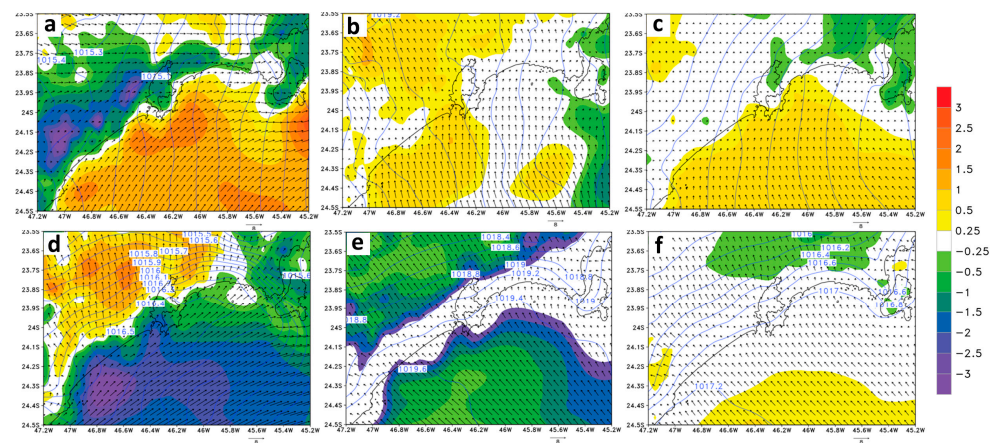

Figure 6. The three local conditions favorable to the occurrence of storm surges: 10 m wind vectors, wind strength difference between future and reference climates(shading), and the PNMM (isolines). The average of the future climate is for the period 2031–2060, at 06Z (**a–c**) and 18Z (**d–f**): Pattern 1 (first column); Pattern 2 (second column); and Pattern 3 (third column).

In Pattern 1, the direction winds are predominant from the southwest, creating a fetch wind parallel to the coast, supporting storm surge days. There is an increase in the wind speed at 06Z (Figure 6a) while it decreases at 18Z (Figure 6d) over the coastline.

In Pattern 2, at 06Z (Figure 6b), the winds blow from the south, and there is an increase in the wind speed over the coastline, contributing to storm surge events. On the other hand, at 18Z (Figure 6e), the winds are from the southeast and are weaker than in the reference climate over the coastal region.

In Pattern 3, there is an increase in wind speed over the ocean, including all the coastline, at 06Z (Figure 6c). There are no evident changes in wind speed, near the coast, at 18Z (Figure 6f).

In general, all projections show an increase in wind speed over the ocean at 06Z to climate future, but a reduction at 18Z. As the stronger winds mostly occur at 18Z in the reference climate, this weakening of the winds may suggest a weakening of the storm surges. Pattern 1 presents the most significant changes with respect to the reference climate.

Precipitation

The precipitation in the three patterns favors storm surges projected for the climate future (2031–2060) over the RCP8.5 scenario by the 5 km Eta-BESM are shown in Figure 7.

Pattern 1 (Figure 7a) presents a reduction in storm surge days in the future from 6 to 1 potential day. Despite that, this pattern is associated with more intense rains in the future climate. Therefore, it can cause significant damage to the city of Santos and the port area. Projections show that rainfall is intense throughout the coastal region, with values between 18 and 21 mm/day. The highest rainfall values are over the ocean, with values greater than 27 mm/day.
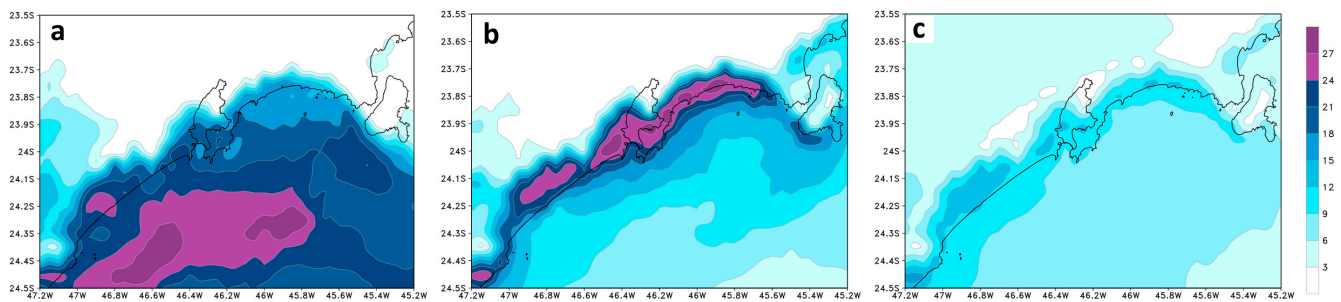
Figure 7. The three rainfall patterns favorable to the occurrence of storm surges projected by the 5 km Eta-BESM during the future climate (2031–2060) in May over the city of Santos: (**a**) Pattern 1; (**b**) Pattern 2; (**c**) and Pattern 3.

Pattern 2 (Figure 7b) has more rain towards the continent. The precipitation is concentrated throughout the São Paulo coastline, reaching values above 27 mm/day. There is an increase in rainfall concerning the present climate. Therefore, the region becomes more vulnerable to impacts, such as landslides and floods.

Pattern 3 (Figure 7c) has 57 potential storm surge days. This pattern could show better changes. There is an increase in rainfall in some parts of the coastal region and a decrease in the ocean. Pattern 3 is characterized by being the one with the highest occurrence; however, it is the least intense in terms of precipitation.

In general, climate projections show an increase in rainfall to climate future in the three patterns over the coastal region.

4. Discussion

The simulations show an overestimated wind speed in the reference climate compared to the ERA5 Reanalysis results from [7]. In addition, the Eta model simulated more potential storm surge days in Pattern 3 and fewer days in Pattern 1. Therefore, the distribution of simulated days among the three patterns corresponds to the same distribution from [7]. These results show satisfactory performance in reproducing the atmospheric patterns required to storm surges by the 20 km Eta-BESM.

The Santos coast is influenced by the passage of frontal systems, the breeze circulation, and the orographic effect. In Figure 4, the times of 06Z and 18Z are shown to emphasize the breeze circulation. At the time of 06Z, there is a land breeze, and the air flows from the continent toward the ocean, with high pressures over the continent and lower pressures over the ocean. Despite this, due to the performance of synoptic scale systems in storm surge events, such as cyclones and anticyclones, the effects of these circulations overlap the circulation of the breeze. Therefore, at 06Z, the forcing of the surface mesoscale circulation is contrary to the large-scale flow, causing a deceleration of the winds towards the coast. On the other hand, at 18Z time, there is the presence of sea breeze; the air blows from the ocean to the continent, with the highest-pressure values over the sea and lowest. Thus, the forcing of the surface sea breeze circulation favors large-scale flow.

Pattern 1 is characterized, on a synoptic scale, by the presence of a cyclone over the ocean with winds parallel to the coast. In the dynamic downscaling at 5 km, the winds from the southwest are weaker at 06Z due to the forcing of the land breeze circulation, which presents winds in the opposite direction to the large-scale flow. At 18Z, there is a center of high pressure on the coast, contributing to the acceleration of surface flow towards the coastal region, accelerating the winds that enter the continent.

Pattern 2 stands out for presenting an intense southeast wind track formed by the presence of an anticyclone and a cyclone over the ocean, which extends to the coastal region of Santos. The flow of 06Z shows higher wind intensities 10 m close to the coast, reaching values greater than 9 m/s. The prevailing wind directions are from the south and southeast, prevailing the action of the large-scale circulation.

Pattern 3 is the most frequent and favorable to storm surges. This pattern is characterized by winds parallel to the coast coming from the center of high pressure, on a synoptic scale, over the continent. On a local scale, at 06Z, the southwest winds weaken as they approach the coastal zone, which may occur due to the roughness of the topography that acts to slow them down. At 18Z, the winds are from the southeast, favored by the sea breeze.

These atmospheric conditions were already observed on the Santos coast by the authors of [10]. These authors evaluated the atmospheric influence over the ocean for storm surge events along the coast. The authors concluded that these extreme events occur due to the migration and persistence of extratropical cyclones with wind speeds greater than 8 m/s near the coastline.

These patterns are also found in [38,39] in other areas on the southern coast of South America. Ref. [39] investigated the oceanic and atmospheric features of an extreme cyclone that generated high waves in southern Brazil. These authors concluded that the anticyclone position relative to the cyclone centers plays a crucial role in storm surge intensity due to the increase in the horizontal pressure gradient and, consequently, the increase in the wind speed. Moreover, the continental anticyclone affects the cyclone's travel speed, which affects the extension and position of the wind fetch.

The climate projections show a similar number of potential storm surge days to Patterns 2 and 3 simulated by the scenarios RCP4.5 and RCP8.5. The RCP8.5 presents 6 and 77 days in Patterns 2 and 3, respectively, whereas RCP4.5 shows 7 and 78 days. In Pattern 1, the RCP4.5 scenario indicates a wind speed stronger than RCP8.5 near the coast and a more intense center of low pressure over the ocean. Regarding the reference climate, both scenarios show wind speeds more intense in Pattern 1 and less severe in Patterns 2 and 3.

The changes at the local scale show the increased wind intensity along the coastline, at 06Z, in all patterns. In contrast, negative anomalies indicate weaker winds at 18Z, mainly in Patterns 1 and 2. Pattern 3 does not show evident changes in the future.

Observed impacts of climate change include increased rainfall intensity that causes instability in coastal areas, including cities, that suffer from flooding and landslides. In the long term, this phenomenon is associated with increased storms and winds, which may increase storm surges. The 5 km Eta-BESM projections showed intense precipitation throughout the coastline. The highest rainfall values are verified over the ocean in Pattern 1. In Patterns 2 and 3, precipitation is concentrated along the entire coast of Santos. The projections of the three patterns indicate increased rainfall in the Santos region. These patterns will become more intense and can cause significant damage to the city of Santos.

5. Conclusions

The city of Santos' vulnerability to variability and climate change is associated with high population density and intense economic activity. Therefore, the coastal city of Santos requires investments and measures to adapt to climate change, reducing risks and minimizing impacts caused by extreme climatic and oceanographic events observed in the present and projected for the future. The main objective of this work was to characterize changes in meteorological conditions favorable to the occurrence of storm surges based on future climate projections for the city of Santos.

The detection scheme showed that the 20 km Eta-BESM reproduced the observed atmospheric patterns favorable to storm surges found in [7]. The simulation underestimated the number of cases in Pattern 1 and Pattern 2. However, it overestimated the number of days in Pattern 3. In general, 20 km Eta-BESM presented more intense winds over the ocean in the three patterns compared to the ERA5 Reanalysis. Despite this, the atmospheric conditions of the three patterns were spatially configured adequately.

In conclusion, the storm surge events characterized by Pattern 1 will become more intense. However, it will be equal to or less frequent than the reference climate. In Pattern 2, both scenarios point to a decrease in the number of events in the future. Nevertheless, these episodes will be associated with more precipitation along the coastline. The heavy rain associated with increased storms and winds can result in a higher intensity of storm surges. Finally, Pattern 3

will have a similar number of storm surge events in the future. However, the winds will tend to be weaker.

References

1. Muis, S.; Verlaan, M.; Winsemius, H.C.; Aerts, J.C.J.H.; Ward, P.J. A Global Reanalysis of Storm Surges and Extreme Sea Levels. *Nat. Commun.* **2016**, *7*, 11969. [CrossRef] [PubMed]
2. Pugh, D.T. *Tides, Surges and Mean Sea-Level (Reprinted with Corrections)*; John Wiley & Sons Ltd.: Hoboken, NJ, USA, 1996; Volume 5.
3. Alfredini, P.; Arasaki, E.; Pezzoli, A.; Arcorace, M.; Cristofori, E.; de Sousa, W.C. Exposure of Santos Harbor Metropolitan Area (Brazil) to Wave and Storm Surge Climate Changes. *Water Qual. Expo. Health* **2014**, *6*, 73–88. [CrossRef]
4. Reboita, M.S.; da Rocha, R.P.; de Souza, M.R.; Llopart, M. Extratropical Cyclones over the Southwestern South Atlantic Ocean: HadGEM2-ES and RegCM4 Projections. *Int. J. Climatol.* **2018**, *38*, 2866–2879. [CrossRef]
5. Ji, T.; Li, G.; Liu, R. Historical Reconstruction of Storm Surge Activity in the Southeastern Coastal Area of China for the Past 60 Years. *Earth Space Sci.* **2020**, *7*, e2019EA001056. [CrossRef]
6. Lai, Y.; Li, Q.; Li, J.; Zhou, Q.; Zhang, X.; Wu, G. Evolution of Frequency and Intensity of Concurrent Heavy Precipitation and Storm Surge at the Global Scale: Implications for Compound Floods. *Front. Earth. Sci.* **2021**, *9*, 660359. [CrossRef]
7. Sondermann, M.; Chou, S.C.; Souza, C.R.d.G.; Rodrigues, J.; Caprace, J.D. Atmospheric Patterns Favourable to Storm Surge Events on the Coast of São Paulo State, Brazil. *Nat. Hazards* **2023**, *117*, 93–111. [CrossRef]
8. Hersbach, H.; Bell, B.; Berrisford, P.; Hirahara, S.; Horányi, A.; Muñoz-Sabater, J.; Nicolas, J.; Peubey, C.; Radu, R.; Schepers, D.; et al. The ERA5 Global Reanalysis. *Q. J. R. Meteorol. Soc.* **2020**, *146*, 1999–2049. [CrossRef]
9. Souza, C.R.d.G.; Souza, A.P.; Harari, J. Long Term Analysis of Meteorological-Oceanographic Extreme Events for the Baixada Santista Region. In *Climate Change in Santos Brazil: Projections, Impacts and Adaptation Options*; Springer International Publishing: Cham, Switzerland, 2019; pp. 97–134.
10. Campos, R.M.; De Camargo, R.; Harari, J. Caracterização de Eventos Extremos Do Nível Do Mar Em Santos e Sua Correspondência Com as Reanálises Do Modelo Do NCEP No Sudoeste Do Atlântico Sul. *Rev. Bras. Meteorol.* **2010**, *25*, 175–184. [CrossRef]
11. Bashmakov, I.; Nilsson, L.; Acquaye, A.; Bataille, C.; Cullen, J.; de la Rue du Can, S.; Fischedick, M.; Geng, Y.; Tanaka, K. Climate Change 2022: Mitigation of Climate Change. In *Contribution of Working Group III to the Sixth Assessment Report of the Intergovernmental Panel on Climate Change*; Chapter 11; E-Scholarship Repository: Berkeley, CA USA, 2022.
12. Chou, S.-C.; Marengo, J.A.; Silva, A.J.; Lyra, A.A.; Tavares, P.; Souza, C.R.D.G.; Harari, J.; Nunes, L.H.; Greco, R.; Hosokawa, E.K.; et al. Projections of Climate Change in the Coastal Area of Santos. In *Climate Change in Santos Brazil: Projections, Impacts and Adaptation Options*; Springer International Publishing: Cham, Switzerland, 2019; pp. 59–73.
13. Veiga, S.F.; Nobre, P.; Giarolla, E.; Capistrano, V.; Baptista, M., Jr.; Marquez, A.L.; Figueroa, S.N.; Bonatti, J.P.; Kubota, P.; Nobre, C.A. The Brazilian Earth System Model Ocean–Atmosphere (BESM-OA) Version 2.5: Evaluation of Its CMIP5 Historical Simulation. *Geosci. Model Dev.* **2019**, *12*, 1613–1642. [CrossRef]
14. Chou, S.C.; Lyra, A.; Mourão, C.; Dereczynski, C.; Pilotto, I.; Gomes, J.; Bustamante, J.; Tavares, P.; Silva, A.; Rodrigues, D.; et al. Evaluation of the Eta Simulations Nested in Three Global Climate Models. *Am. J. Clim. Chang.* **2014**, *3*, 438–454. [CrossRef]

15. Lyra, A.; Tavares, P.; Chou, S.C.; Sueiro, G.; Dereczynski, C.; Sondermann, M.; Silva, A.; Marengo, J.; Giarolla, A. Erratum to: Climate Change Projections over Three Metropolitan Regions in Southeast Brazil Using the Non-Hydrostatic Eta Regional Climate Model at 5-Km Resolution. *Theor. Appl. Climatol.* **2018**, *132*, 663–682. [CrossRef]

16. Zanetti, V.B.; Júnior, W.C.d.S.; Hosokawa, E.K. Vulnerability of Critical Infrastructure Under Climate Change Scenarios: The Case of Santos. In *Climate Change in Santos Brazil: Projections, Impacts and Adaptation Options*; Springer International Publishing: Cham, Switzerland, 2019; pp. 245–251.

17. Santos, B.B.d.O.; Nunes, L.H.; Bandini, M.P. Rainfall Episodes and Local Stability Thresholds in Santos. In *Climate Change in Santos Brazil: Projections, Impacts and Adaptation Options*; Springer International Publishing: Cham, Switzerland, 2019; pp. 161–175.

18. Mesinger, F. A Blocking Technique for Representation of Mountains in Atmospheric Models. *Riv. Meteorol. Aeronaut.* **1984**, *44*, 195–202.

19. Mesinger, F.; Chou, S.C.; Gomes, J.L.; Jovic, D.; Bastos, P.; Bustamante, J.F.; Lazic, L.; Lyra, A.A.; Morelli, S.; Ristic, I.; et al. An Upgraded Version of the Eta Model. *Meteorol. Atmos. Phys.* **2012**, *116*, 63–79. [CrossRef]

20. Mesinger, F.; Veljovic, K.; Chou, S.C.; Gomes, J.; Lyra, A. The Eta Model: Design, Use, and Added Value. In *Topics in Climate Modeling*; InTech: New Delhi, India, 2016.

21. Marengo, J.A.; Chou, S.C.; Kay, G.; Alves, L.M.; Pesquero, J.F.; Soares, W.R.; Santos, D.C.; Lyra, A.A.; Sueiro, G.; Betts, R.; et al. Development of Regional Future Climate Change Scenarios in South America Using the Eta CPTEC/HadCM3 Climate Change Projections: Climatology and Regional Analyses for the Amazon, São Francisco and the Paraná River Basins. *Clim. Dyn.* **2012**, *38*, 1829–1848. [CrossRef]

22. Chou, S.C.; Marengo, J.A.; Lyra, A.A.; Sueiro, G.; Pesquero, J.F.; Alves, L.M.; Kay, G.; Betts, R.; Chagas, D.J.; Gomes, J.L.; et al. Downscaling of South America Present Climate Driven by 4-Member HadCM3 Runs. *Clim. Dyn.* **2012**, *38*, 635–653. [CrossRef]

23. Pesquero, J.F.; Chou, S.C.; Nobre, C.A.; Marengo, J.A. Climate Downscaling over South America for 1961-1970 Using the Eta Model. *Theor. Appl. Climatol.* **2010**, *99*, 75–93. [CrossRef]

24. Janjic, Z.I.; Gerrity, J.; Nickovic, S. An Alternative Approach to Nonhydrostatic Modeling. *Mon. Weather Rev.* **2001**, *129*, 1164–1178. [CrossRef]

25. Janjic, Z.I. Forward-Backward Scheme Modified to Prevent Two-Grid-Interval Noise and Its Application in Sigma Coordinate Models. *Contrib. Atmos. Phys* **1979**, *52*, 69–84.

26. Janjic, Z.I. Nonlinear Advection Schemes and Energy Cascade on Semi-Staggered Grids. *Mon. Weather Rev.* **1984**, *112*, 1234–1245. [CrossRef]

27. Betts, A.K.; Miller, M.J. A New Convective Adjustment Scheme. Part II: Single Column Tests Using GATE Wave, BOMEX, ATEX and Arctic Air-mass Data Sets. *Q. J. R. Meteorol. Soc.* **1986**, *112*, 693–709. [CrossRef]

28. Zhao, Q.; Carr, F.H. A Prognostic Cloud Scheme for Operational NWP Models. *Mon. Weather Rev.* **1997**, *125*, 1931–1953. [CrossRef]

29. Schwarzkopf, M.D.; Fels, S.B. The Simplified Exchange Method Revisited: An Accurate, Rapid Method for Computation of Infrared Cooling Rates and Fluxes. *J. Geophys. Res.* **1991**, *96*, 9075. [CrossRef]

30. Lacis, A.A.; Hansen, J. A Parameterization for the Absorption of Solar Radiation in the Earth's Atmosphere. *J. Atmos. Sci.* **1974**, *31*, 118–133. [CrossRef]

31. Paulson, C.A. The Mathematical Representation of Wind Speed and Temperature Profiles in the Unstable Atmospheric Surface Layer. *J. Appl. Meteorol.* **1970**, *9*, 857–861. [CrossRef]

32. Ek, M.B.; Mitchell, K.E.; Lin, Y.; Rogers, E.; Grunmann, P.; Koren, V.; Gayno, G.; Tarpley, J.D. Implementation of Noah Land Surface Model Advances in the National Centers for Environmental Prediction Operational Mesoscale Eta Model. *J. Geophys. Res. Atmos.* **2003**, *108*, 2002JD003296. [CrossRef]

33. Nakanishi, M.; Niino, H. Development of an Improved Turbulence Closure Model for the Atmospheric Boundary Layer. *J. Meteorol. Soc. Jpn.* **2009**, *87*, 895–912. [CrossRef]

34. Nobre, P.; Siqueira, L.S.P.; de Almeida, R.A.F.; Malagutti, M.; Giarolla, E.; Castelão, G.P.; Bottino, M.J.; Kubota, P.; Figueroa, S.N.; Costa, M.C.; et al. Climate Simulation and Change in the Brazilian Climate Model. *J. Clim.* **2013**, *26*, 6716–6732. [CrossRef]

35. Reboita, M.S.; Gan, M.A.; da Rocha, R.P.; Ambrizzi, T. Regimes de Precipitação Na América Do Sul: Uma Revisão Bibliográfica. *Rev. Bras. De Meteorol.* **2010**, *25*, 185–204. [CrossRef]

36. Beck, H.E.; van Dijk, A.I.J.M.; Levizzani, V.; Schellekens, J.; Miralles, D.G.; Martens, B.; de Roo, A. MSWEP: 3-Hourly 0.25° Global Gridded Precipitation (1979–2015) by Merging Gauge, Satellite, and Reanalysis Data. *Hydrol. Earth Syst. Sci.* **2017**, *21*, 589–615. [CrossRef]

37. Zheng, F.; Westra, S.; Sisson, S.A. Quantifying the Dependence between Extreme Rainfall and Storm Surge in the Coastal Zone. *J. Hydrol.* **2013**, *505*, 172–187. [CrossRef]

38. Dragani, W.C.; Cerne, B.S.; Campetella, C.M.; Possia, N.E.; Campos, M.I. Synoptic Patterns Associated with the Highest Wind-Waves at the Mouth of the Río de La Plata Estuary. *Dyn. Atmos. Ocean.* **2013**, *61*, 1–13. [CrossRef]

39. Gramcianinov, C.B.; Campos, R.M.; Guedes Soares, C.; de Camargo, R. Extreme Waves Generated by Cyclonic Winds in the Western Portion of the South Atlantic Ocean. *Ocean Eng.* **2020**, *213*, 107745. [CrossRef]